

1 Imprint of relative sea-level histories on Last 2 Interglacial coral preservation

3
4 R. Cleveland Stout¹, T. Pico², P. Huybers³, J.X. Mitrovica³, and J. Austermann⁴

5 ¹ Department of Atmospheric Sciences, University of Washington, Seattle, WA, USA

6 ² Department of Earth and Planetary Sciences, University of California-Santa Cruz, Santa Cruz, CA, USA

7 ³ Department of Earth and Planetary Sciences, Harvard University, Cambridge, MA, USA

8 ⁴ Department of Earth and Environmental Sciences, Lamont-Doherty Earth Observatory, Columbia University,
9 Palisades, NY, USA

10 Received 2023 January 9; in original form 2023 January 9

11 Imprint of relative sea-level histories on LIG coral preservation

12 Corresponding author: Rebecca Cleveland Stout (rccs@uw.edu)

13
14
15
16

17 **SUMMARY**

18 Fossil corals are commonly used to reconstruct Last Interglacial (~125 ka, LIG) sea level. Sea-
19 level reconstructions assume the water depth at which the coral lived, called the “relative water
20 depth”. However, relative water depth varies in time and space due to coral reef growth in
21 response to relative sea-level (RSL) changes. RSL changes can also erode coral reefs, exposing
22 older reef surfaces with different relative water depths. We use a simplified numerical model of
23 coral evolution to investigate how sea-level history systematically influences the preservation of
24 corals in the Bahamas and western Australia, regions which house >100 LIG coral fossils. We
25 construct global ice histories spanning the uncertainty of LIG global mean sea level (GMSL) and
26 predict RSL with a glacial isostatic adjustment model. We then simulate coral evolution since
27 132 ka. We show that preserved elevations and relative water depths of modeled LIG corals are
28 sensitive to the magnitude, timing, and number of GMSL highstand(s). In our simulations, the
29 influence of coral growth and erosion (i.e., the “growth effect”) can have an impact on RSL
30 reconstructions that is comparable to glacial isostatic adjustment. Thus, without explicitly
31 accounting for the growth effect, additional uncertainty is introduced into sea-level
32 reconstructions. Our results suggest the growth effect is most pronounced in western Australia
33 due to Holocene erosion, but also plays a role in the Bahamas, where LIG RSL rose rapidly due
34 to the collapsing peripheral bulge associated with Laurentide Ice Sheet retreat. Despite the coral
35 model’s simplicity, our study highlights the utility of process-based RSL reconstructions.

36 **Key words:** sea-level change – loading of the Earth – geomorphology – numerical modelling

37 **1 INTRODUCTION**

38 Constraining the pattern and rate of global sea-level change during the Last Interglacial
39 (LIG; ~128–116 ka; Rovere et al., 2016) offers insight into ice sheet sensitivity to temperature
40 forcing, which underpins future sea-level rise projections (e.g., DeConto et al., 2021). Fossil
41 corals are widely used to reconstruct LIG sea level, as they grow close to the sea surface and can
42 be accurately dated using U-series methods (Chutcharavan & Dutton, 2021; Stirling & Andersen,
43 2009). Sea-level reconstructions based on fossil coral reefs estimate that global mean sea level
44 (GMSL) during the LIG peaked at 5.5–9 m (Dutton & Lambeck, 2012; Kopp et al., 2009) or less
45 (Dyer et al., 2021) above the present day. However, significant debate surrounds the timing,
46 duration, number, and magnitude of the highstand(s) (e.g., Barlow et al., 2018; Dyer et al., 2021;
47 Kopp et al., 2013; Neumann & Hearty, 1996; Stirling et al., 1995, 1998; Thompson et al., 2011).

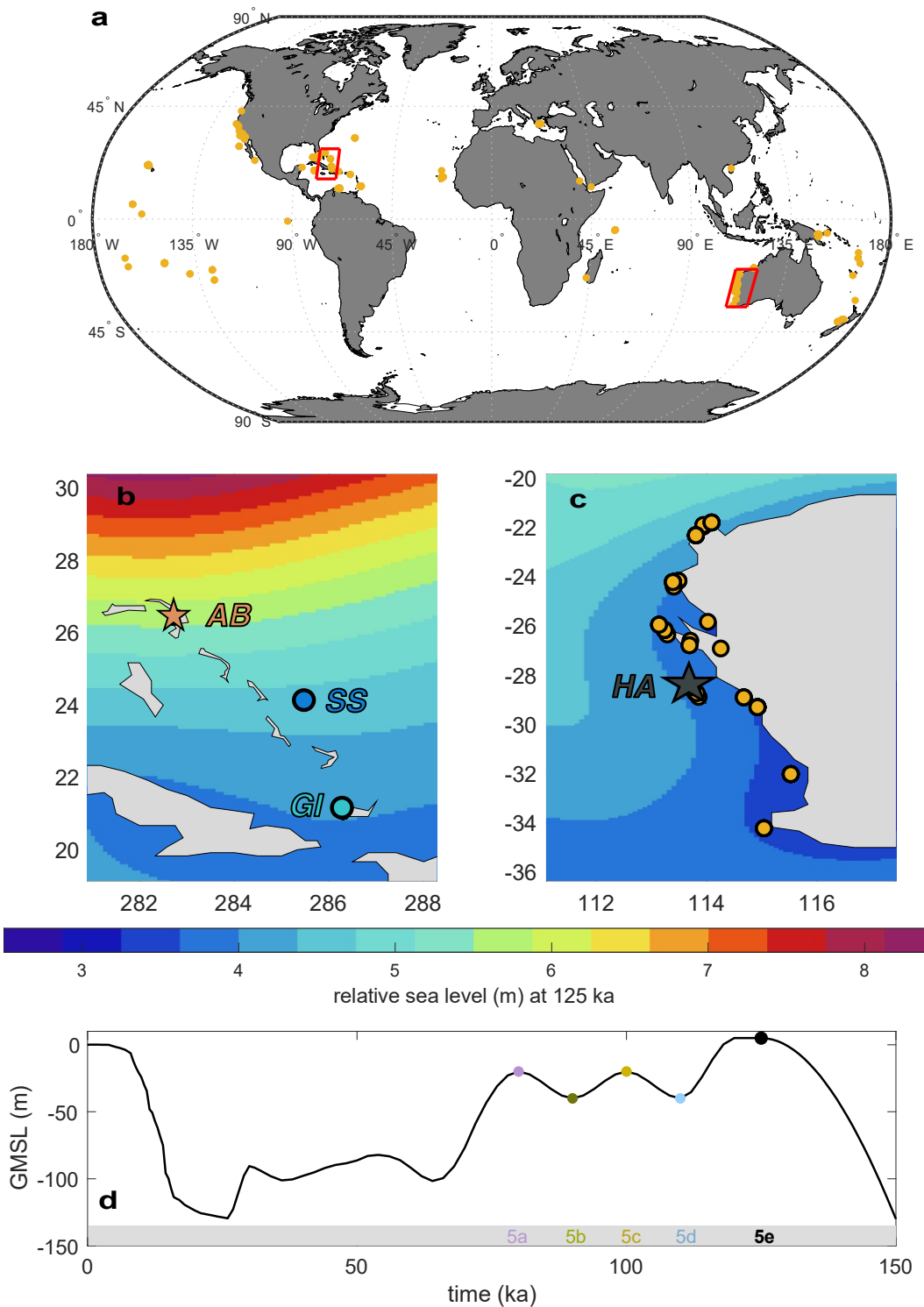
48 Coral growth is highly dependent on the coral’s depth below the sea surface, and thus is
49 influenced by rates of sea-level change. Although growth rates vary by species, coral growth is
50 dependent on light availability (Hopley, 2011) such that the rate of vertical coral accretion can,
51 for many species, be approximated as a decreasing logarithmic function of depth (Kleypas,
52 1997). The maximum coral reef accretion rate is species dependent, but often occurs around 5 m
53 depth, where wave stress is low and light availability is high (Woodroffe & Webster, 2014). As
54 sea level rises, a coral may continue growing to keep up with sea level (Hopley, 2011), but will
55 die if the long-term rate of sea-level rise exceeds the long-term vertical accretion rate. When sea
56 level falls, a coral may be eroded due to wave action (Toomey et al., 2013).

57 Sea-level reconstructions using coral reefs rely on the relative water depth (also referred
58 to as the indicative meaning), which is an assumption of how far below the mean lower low
59 water the coral reef grew. This value is often based on modern coral depth distributions (e.g.,

60 Hibbert et al., 2016). Typically, the mean relative water depth and a corresponding uncertainty is
61 added to the present-day coral fossil elevation to reconstruct relative sea level at the time of
62 interest, when the coral reef was alive (e.g., Rovere et al., 2016). However, this approach
63 assumes a relative water depth for a given reef that is constant through time and space. It thus
64 fails to account for how coral growth may influence the relative water depth in response to
65 spatially varying sea-level change, and how coral erosion may expose coral reef surfaces with
66 older ages and different relative water depths. Prior studies have used LIG coral erosional
67 surfaces and reef growth patterns to assess sea-level highstands or trends of sea-level rise and fall
68 at a given location (e.g., de Gelder et al., 2022; O’Leary et al., 2013; Skrivanek et al., 2018).
69 Forward numerical models of coral reefs have also been used to better understand the impact of
70 sea-level oscillations on reef growth and preservation at one or two individual locations (Boyden
71 et al., 2023; de Gelder et al., 2022; Pastier et al., 2019). Nevertheless, the integrated coral growth
72 and erosion history over an entire glacial cycle and across locations has not yet been
73 systematically considered.

74 Because corals are sensitive to sea-level change, understanding coral growth, erosion, and
75 ultimate preservation resulting from a range of possible LIG global ice volume scenarios can
76 provide insight into a coral’s ability to record local LIG sea level. In this study, we simulate coral
77 growth and erosion in response to sea-level change using a simple coral parameterization to
78 model the formation and preservation of LIG corals in the Bahamas and western Australia,
79 regions which house a large number ($n > 100$) of LIG fossil corals and experienced different
80 relative sea level (RSL) histories over the last glacial cycle given their respective location in
81 relation to past former ice sheets (Dendy et al., 2017; Figure 1). Since the history of global sea-
82 level change is uncertain, we explore a broad range of possible scenarios over the LIG by

83 varying the magnitude, timing, and pattern of peak GMSL. Our goal is not to robustly constrain
84 LIG sea-level or interpret specific fossil coral reef records; rather, we seek to discover how coral
85 growth and erosion interplays with relative sea-level change across the Bahamas and western
86 Australia to produce present-day preserved LIG coral fossil elevations. Quantifying this
87 relationship may provide additional insight into the ability of preserved present-day corals to
88 capture local LIG sea level, as different patterns of local LIG sea-level change may influence a
89 coral's depth below the sea surface, as well as the uncertainty associated with coral-based sea-
90 level reconstructions.



91

92

93

Figure 1. Map of Last Interglacial corals and relative sea level at 125 ka. Locations of coral fossils dated to the LIG are shown in yellow, and the Bahamas and western Australia are indicated with red boxes (a).

94 Insets show relative sea level at 125 ka in the Bahamas (b) and western Australia (c) predicted using a
 95 GIA simulation with the GMSL history shown in (d). In the Bahamas (b), the site at Hole in the Wall,
 96 Abaco Island is starred. All sites in the Bahamas are labeled (Abaco Island, AB; San Salvador Island, SS;
 97 Great Inagua Island, GI), as well as 1 site in western Australia (Houtman Abrolhos Islands, HA). The
 98 GMSL curve (d) has a highstand of +5 m from 125-120 ka, and 125 ka is marked with a dashed vertical
 99 black line. GMSL is interpolated using a piecewise cubic polynomial between +5 m at 120 ka, -40 m at
 100 110 ka (MIS 5d), -20 m at 100 ka (MIS 5c), -40 m at 90 ka (MIS 5b), -20 m at 80 ka (MIS 5a). Points of
 101 interpolation (MIS 5a-d) are indicated with colored circles, and indicated on the x-axis. After 70 ka,
 102 GMSL adopts the deglacial history associated with ICE-5G (Peltier, 2004).

103

104 2 METHODS

105 2.1 Modeling coral growth and erosion in response to sea-level change

106 Our goal is to isolate the effects of sea-level change on coral growth patterns. Thus, we
 107 choose a simplified coral model with growth and erosion rates based on averaged accretion rates
 108 during the LIG of corals in the Pacific, Atlantic, and Indian Oceans (Toomey et al., 2013). The
 109 corals in the LIG dataset (Figure 1a, yellow dots) experienced a complex interplay of processes
 110 besides sea-level change, including inter-species competition, substrate availability, observation
 111 bias, spatially heterogeneous wave regimes, and detailed bathymetry (Woodroffe & Webster,
 112 2014), which are not accounted for in our generalized coral model.

113 The model we use is based on the mathematical relationship between coral surface
 114 elevation and vertical accretion rate, first suggested by Bosscher and Schlager (1992) and
 115 updated by Toomey et al. (2013) to include the effects of tidal depth. For each time-step ($\Delta t =$
 116 10 years), the model calculates the vertical accretion rate of existing live corals in response to

117 local sea-level change $\frac{ds}{dt}$, which is comprised of a GMSL change signal and a GIA signal. The
 118 vertical growth or erosion rate ($\frac{dz}{dt}$) is described by:

119

$$\frac{dz}{dt} = \begin{cases} G_{max} \tanh \left(4.4 \left(1 - \frac{D}{S-Z} \right) \right) - W, & Z > Z_L \\ 0, & Z \leq Z_L \end{cases} \quad (1)$$

$$W = \begin{cases} W_{max}, & s_- \leq Z \leq s_+ \\ W_{max} - 0.1 \text{ m}^{-1} * W_{max}Z, & Z \leq s_-, Z \geq s_+ \end{cases} \quad (2)$$

120 Here, Z is the coral elevation [m]; G_{max} is the maximum vertical accretion rate [m yr^{-1}]; the
 121 constant, 4.4, is an averaged $\frac{I_0}{I_k}$ where I_0 is surface light intensity and I_k is saturating light
 122 intensity [unitless]; D is tidal depth (mean tidal range) [m]; W is erosion [m yr^{-1}]; and s_+ and s_-
 123 are the positive (above the sea surface) and negative (below the sea surface) boundaries for the
 124 surf zone. The values for the parameters adopted in this study are shown in Table 1.

125 **Table 1.** Coral model parameters. Values used for each parameter adopted in the 1D coral model, along
 126 with references for chosen values.

Parameter	Value	Reference
Erosion (W_{max})	0.5 mm/year	Kleypas (1997)
Tidal depth (D)	1.15 m (Bahamas); 1.50 m (Western Australia)	Hibbert et al. (2016)
Maximum vertical accretion (G_{max})	4.5 mm/year	Toomey et al. (2013); Kleypas (1997)
Surf zone (s)	-3 to 2.4 m	Hearn (1999)
Initiation time (t_0)	132 ka	----
Limiting depth (Z_L)	-20 m	Hibbert et al. (2016)
Surface light intensity divided by	4.4	Bosscher and Schlager (1992)

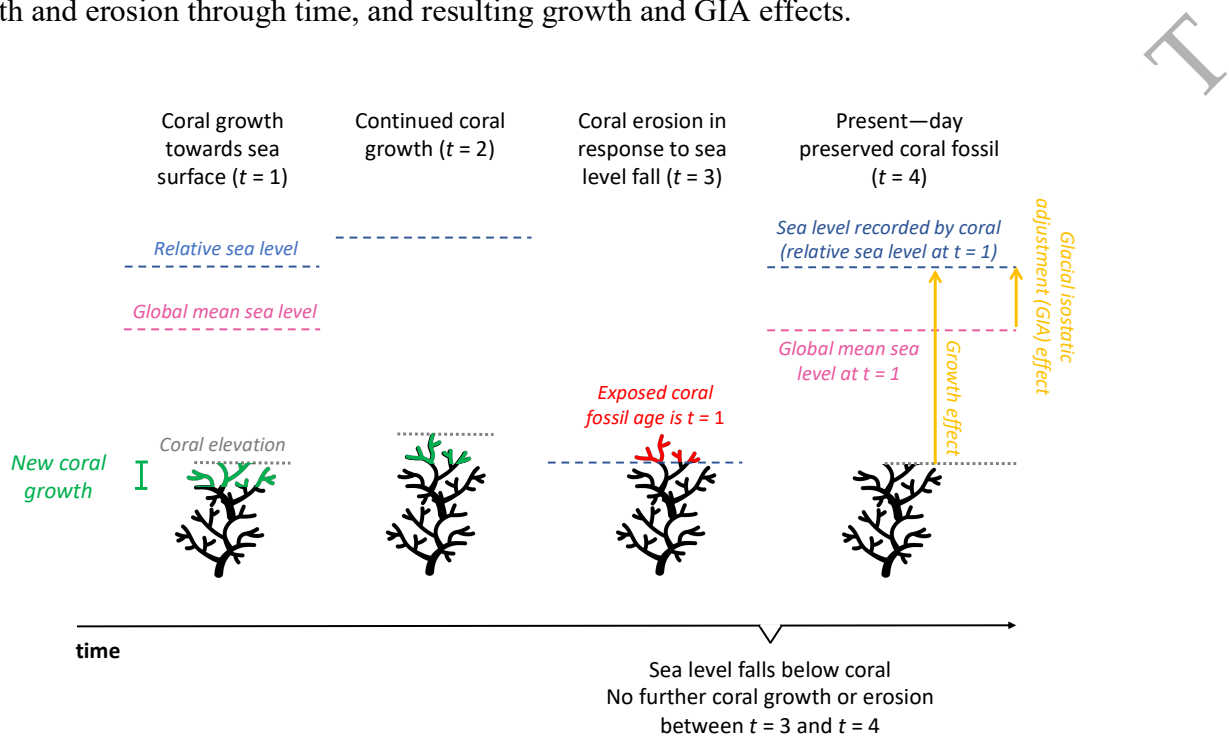
saturating light
intensity (I_0 / I_k)

127

128 We initialize coral models at 132 ka (~2-7 ka before the peak LIG GMSL). This assumes
 129 that sea-surface temperatures in western Australia and the Bahamas at this time were similar to
 130 present, allowing for coral growth (Hoffman et al., 2017). We simulate a single reef in each grid
 131 cell with observed LIG corals ($0.35^\circ \times 0.35^\circ$ resolution). Simulated corals are placed at the tidal
 132 depth associated with sea level at the initiation time (see Table 1). Coral growth occurs when the
 133 coral is underwater ($Z < 0$), and corals stop growing when their elevation falls below a threshold
 134 called the limiting depth ($Z < Z_L$) or when the rate of vertical accretion is less than the rate of
 135 sea-level rise ($\frac{dZ}{dt} < \frac{dS}{dt}$) (Kleypas, 1997; Toomey et al., 2013). If corals are exposed subaerially (Z
 136 > 0), corals stop growing, and coral growth is re-initiated when corals are re-submerged. After
 137 each simulation, the age of the modeled corals are calculated as the time at which the exposed
 138 coral surface was last in growth position (i.e., the most recent time when $Z < 0$). The RSL
 139 recorded by the coral (i.e., RSL at the time the coral was most recently growing) is then
 140 calculated as the RSL at that time (see Fig. 2).

141 We then identify the impacts of dynamic coral growth and GIA on modeled present-day
 142 elevations of LIG coral fossils. We define the *growth effect* as the RSL recorded by the coral
 143 subtracted from the present-day coral elevation, which is equivalent to the water depth at which
 144 the coral grew. We define the *GIA effect* as the GMSL subtracted from the RSL recorded by the
 145 coral. The growth effect thus includes coral growth and erosion in response to sea-level changes,
 146 and the GIA effect does not. The growth effect is always negative because our model does not
 147 permit coral growth above the sea surface. Thus, the present-day elevation of the coral is the

148 RSL recorded by the coral plus the (negative) growth effect. The growth effect has a maximum
 149 value of tidal depth (-1.15 m in the Bahamas, -1.50 m in western Australia); a growth effect at
 150 this value indicates that the coral was fully caught up to LIG RSL at the time of its death. A more
 151 negative growth effect indicates that the coral was not caught up with RSL at the time of its
 152 death, and tidal depth cannot be used to reconstruct RSL. Figure 2 shows a schematic of coral
 153 growth and erosion through time, and resulting growth and GIA effects.



154
 155 **Figure 2.** Schematic of coral growth in response to sea-level rise and fall. Schematic shows coral at 4
 156 timesteps: ($t = 1$) coral with upward growth (green) towards sea surface since initialization at $t = 0$; ($t =$
 157 2) coral with continued upward growth (green) towards sea surface; ($t = 3$) eroding coral (red) in response
 158 to sea-level fall; and ($t = 4$) coral fossil at present-day, with eroded coral removed from the top. Relative
 159 sea level is shown with dashed blue lines, and coral elevation at each timestep is indicated with dotted
 160 grey lines. The exposed coral fossil at present-day ($t = 4$) is dated to $t = 1$, and therefore the relative sea
 161 level that is recorded by the coral is relative sea level at $t = 1$. Relative sea level at $t = 1$ (blue dashed line)
 162 minus global mean sea level at $t = 1$ (pink dashed line) is shown in yellow as the vertical glacial isostatic

163 adjustment (GIA) effect. The growth effect (relative sea level recorded by the coral minus coral elevation)
164 is also shown in yellow.

165

166 **2.2 Glacial isostatic adjustment model and global mean sea level over the last glacial cycle**

167 To predict the relative sea-level history for each LIG coral site in the Bahamas and
168 western Australia, we first generate a set of 900 GMSL histories over the last glacial cycle. This
169 allows us to explore impacts of GMSL peak type, peak timing, and peak magnitude on the
170 relative sizes of the growth and GIA effects in the Bahamas and western Australia. We assume
171 that the penultimate glacial maximum had the same GMSL as during the Last Glacial Maximum
172 (-130 m), and that the penultimate deglaciation lasted ~20 kyr (putting the penultimate glacial
173 maximum at 150 ka), although there is evidence that the penultimate deglaciation was shorter
174 than 13 kyr (e.g., P. U. Clark et al., 2020). After pinning the penultimate glacial maximum at 150
175 ka with a GMSL of -130 m, we sample a range of possible GMSL histories during the LIG,
176 based on previously suggested patterns and magnitudes of GMSL change (e.g., Blanchon et al.,
177 2009; Dechnik et al., 2017; Hearty et al., 2007; Kopp et al., 2013; Neumann & Macintyre, 1985;
178 Rohling et al., 2008; Skrivanek et al., 2018; Stirling et al., 1998; Thompson et al., 2011). The
179 peak GMSL magnitude is randomly sampled between 0 and 10 m, where the latter is the 15%
180 probability exceedance value of the LIG GMSL highstand estimated by Kopp et al. (2009). and
181 the lowstands are sampled between -2 m and the lowest sampled GMSL peak for a given run.

182 We also vary the pattern of GMSL during the LIG according to three scenarios: a single
183 GMSL highstand referred to as ‘single peak’ (Figure 3b), a delayed ascending GMSL highstand
184 preceded by a 2 ky period of stability called ‘ascending peak’ (Figure 3c), and a double GMSL

185 highstand separated by 2 ky of lower GMSL, called ‘oscillating peak’ (Figure 3d). In addition,
 186 we vary the timing of the GMSL highstand, which modulates the rate of sea-level change
 187 preceding and following the LIG GMSL highstand (Table 2). Across the LIG (between 130-115
 188 ka), the rate of GMSL change varies from -7.7 to 16.8 m/kyr.

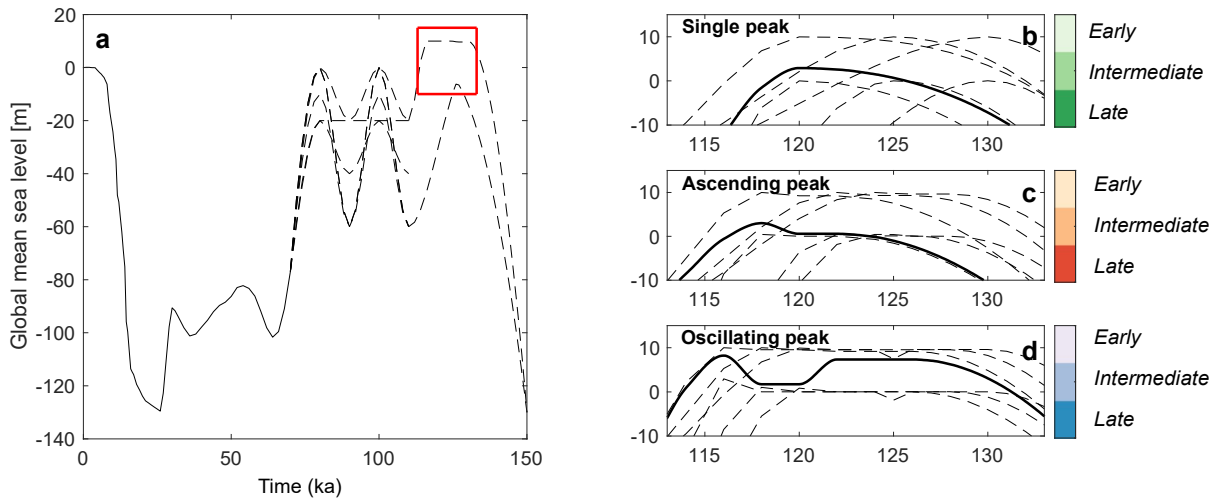
189 **Table 2.** Timing of GMSL peaks used in this study. For the ascending and oscillating peak, the timing of
 190 the initial and final peak is shown. GMSL peaks are sampled between 0 and 10 m. For the oscillating
 191 peak, a GMSL lowstand preceding the second GMSL highstand is sampled between -2m (minimum) and
 192 the height of the previous peak (maximum).

Timing	Single peak	Ascending peak	Oscillating peak
Early	130 ka	128 ka, 124 ka	130 ka, 120 ka
Intermediate	125 ka	126 ka, 122 ka	128 ka, 118 ka
Late	120 ka	124 ka, 120 ka	126 ka, 116 ka

193

194 We sample a range of estimates during MIS 5a-d to populate GMSL history through 70
 195 ka (Figure 3a; Creveling et al., 2017; Cutler et al., 2003). Sea level falls at a rapid, intermediate,
 196 or slow rate to -60, -40, or -20 meters, respectively, during MIS 5d (110 ka). To account for
 197 potential erosion or re-submergence of LIG corals, we vary the magnitude of subsequent GMSL
 198 highstands during MIS 5c (100 ka), although our subsequent analysis only considers modeled
 199 reefs aged 132-115 ka. The GMSL highstand during MIS 5c is either high-, intermediate-, or
 200 low-magnitude, with a value of 0, -10, or -20 meters, respectively. The sampled GMSL values
 201 for MIS 5d and MIS 5c are repeated to fill in the loading history during MIS 5b (90 ka) and MIS
 202 5a (80 ka), respectively (Figure 3a; dashed black lines). We use shape-preserving piecewise
 203 cubic interpolation to fill the GMSL curve between sampled points from 150 ka to 70 ka. From
 204 70 ka until modern day, we adopt the GMSL history associated with the ICE-5G model (Peltier,
 205 2004). While the corals are exposed for much of this period, including this period allows us to

206 account for potential erosion or re-submergence of corals during the late Holocene (~8 ka to
207 present). This is especially important for sites in western Australia, which experienced a local
208 highstand at the end of the last deglaciation phase rather than at present-day. Although previous
209 studies have shown that the GMSL history associated with ICE-5G underestimates sea-level
210 during MIS 3 (Pico et al., 2016), our modeled coral distributions are insensitive to GMSL
211 oscillations below ~ -20 m, the limiting depth in the coral model (see Table 1).



212 **Figure 3.** Ensemble of LIG GMSL histories. (a) Range of sampled GMSL histories. Three patterns of
 213 sea-level change are assumed during the Last Interglacial (a; red box). For each simulation of MIS 5d-a,
 214 only 3 values are sampled (possible histories are shown by dashed lines, 110-80 ka). Every ensemble
 215 member adopts an identical GMSL history from 70 ka to present (solid black line). The possible patterns
 216 of Last Interglacial sea level are (right panels): single peak (b), ascending peak (c), and oscillating peak
 217 (d). For the ascending peak, preceding the final (highest) peak, there is a 2 kyr period of stability. The
 218 different shades of color in each inset (b-c) refer to the timing of the peak highstand(s): early (light
 219 shading), intermediate (medium shading) and late (dark shading) (see Table 2). Bounding values of the
 220 sampled GMSL histories for a given timing and peak type are shown with dashed black lines. For b-d, an
 221 illustrative GMSL curve with late timing is shown in solid black.
 222

223
 224 We then produce a set of ice histories corresponding to the ensemble of 900 GMSL
 225 histories (Figure 3). The ice histories are based on ICE-5G (Peltier, 2004), and assume that ice
 226 geometry prior to 26 ka is identical to ice geometry post-26 ka for the same GMSL value. During
 227 the LIG, when GMSL values exceed present-day GMSL, we uniformly reduce the thickness of
 228 the Antarctic and Greenland ice sheet to produce excess melt consistent with the sampled GMSL
 229 values. There are some limitations to this approach; for example, there is evidence that ice

230 volumes over North America and Eurasia differed between the last glacial maximum and
231 penultimate glacial maximum (Colleoni et al., 2016; Rohling et al., 2017), and subsequent
232 research has also refined the deglacial ice thickness history over North America, Northwestern
233 Eurasia, and Antarctica, resulting in updated global ice histories (e.g., Roy & Peltier, 2015,
234 2018). However, the focus of our analysis is sea level prior to 26 ka, a period characterized by
235 large uncertainties in ice extent and volume (e.g., Dalton et al., 2022), and therefore we do not
236 focus on the impact of different ice geometries on reef development.

237 We reconstruct RSL at each site in the Bahamas and western Australia by performing
238 glacial isostatic adjustment (GIA) simulations with each of the 900 ice loading histories. Our
239 calculations are based on the theory and pseudo-spectral algorithm described by Kendall et al.
240 (2005) with a spherical harmonic truncation at degree 256. These calculations adopt a Maxwell
241 rheology that is incompressible in the fluid limit and include both the impact of load-induced
242 Earth rotation changes on sea level (Milne & Mitrovica, 1996, 1998) and evolving shorelines,
243 where the latter incorporates the evolution of grounded, marine-based ice (e.g., Kendall et al.,
244 2005; Milne et al., 1999).

245 In addition to the history of global ice cover, our predictions require regional models for
246 Earth's viscoelastic structure. The Earth model for the Bahamas is characterized by a lithospheric
247 thickness of 96 km, an upper mantle viscosity of 5×10^{20} Pa s and a lower mantle viscosity of 4×10^{21} Pa s, which is consistent with MIS 5a and 5e sea-level data in the Western North Atlantic
248 and other estimates for Earth structure in this region (Creveling et al., 2017; Potter & Lambeck,
249 2004), although higher viscosity estimates in the upper and lower mantle have been obtained
250 using Holocene data (e.g., Milne & Peros, 2013). The Earth model for western Australia is
251 characterized by a lithospheric thickness of 71 km, an upper mantle viscosity of 5×10^{20} Pa s

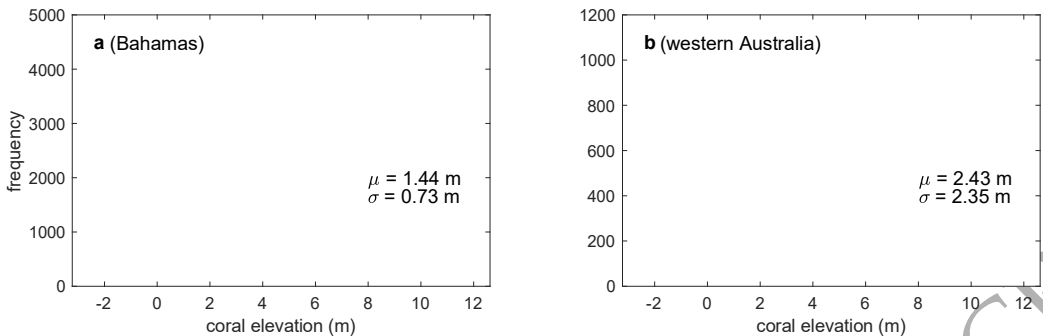
253 and a lower mantle viscosity of 10^{22} Pa s, which is consistent with late Holocene sea-level
254 records in Australia (O’Leary et al., 2013) .

255 To focus on the influence of LIG GMSL histories on coral preservation, we limit our
256 study to a single Earth model for the Bahamas and a single Earth model for western Australia
257 and a single ice history for the penultimate deglaciation extending to 150 ka. Although a suite of
258 900 sea-level histories are produced, we present only a subset, after controlling for peak type,
259 timing, and magnitude.

260 **2.3 Last Interglacial fossil corals in the Bahamas and western Australia**

261 Figure 1a shows a global database of fossil corals (Hibbert et al., 2016). From this
262 database, we compile LIG fossil coral elevations from the Bahamas (77.3-73.7 °W and 21.0-26.4
263 °N) and western Australia (113.1-115.5 °E and 34.2-21.8 °S), two regions characterized by a
264 large sample size ($n > 100$) of LIG fossil corals that have U-series ages between 115-130 ka.
265 Although these regions are widely recognized as passive margin settings, tectonic activity has
266 been observed in western Australia (e.g., Sandstrom et al., 2020). Corals are excluded from the
267 database if they are explicitly listed as not in growth position in the original reference. We note
268 that many of the coral samples do not pass open-system screening requirements (Hibbert et al.,
269 2016), which can bias the ages. In the Bahamas, 155 samples are located among three sites, and
270 in western Australia 102 samples are located among 15 sites (Figure 1b, 1c). To reduce spatial
271 bias in the observed distributions resulting from repeated sampling from the same site, we adopt
272 a sampling frequency based on kriging weights. We use ordinary kriging and a theoretical
273 exponential variogram to calculate these weights, and obtain a sampling frequency by setting the
274 standard deviation of the weights to 20% of the mean, sampling approximately 10,000 times in
275 each region. Coral elevation distributions across the Bahamas and western Australia after

276 sampling are shown in Figure 4a and 4b, respectively. These distributions are markedly different;
 277 for instance, the distribution in western Australia is characterized by a wider range and higher
 278 mean value than that in the Bahamas.



279
 280 **Figure 4.** Distribution of LIG coral elevations. Histograms of present-day elevation distributions of
 281 preserved Last Interglacial coral fossils after sampling according to kriging weights (see text) are shown
 282 for the Bahamas (a) and western Australia (b). Distribution means (μ) and standard deviations (σ) are
 283 displayed.

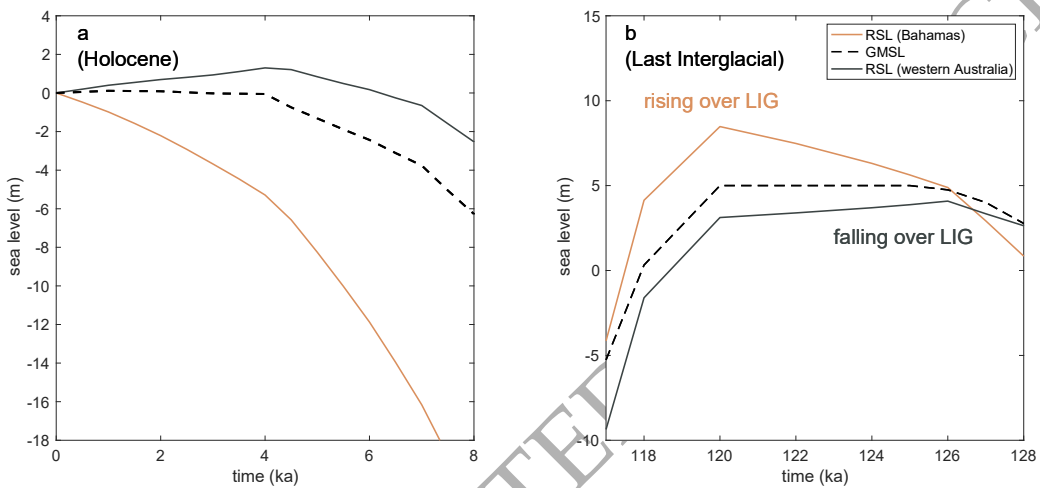
284

285 **3 RESULTS AND DISCUSSION**

286 **3.1 Relative sea level patterns in the Bahamas and western Australia**

287 The Bahamas and western Australia experienced different RSL histories during the LIG
 288 due to GIA (Figure 1). If global mean sea level was stable across the LIG, Western Australia
 289 would experience an early RSL highstand followed by an RSL fall due to the far-field effects of
 290 continental levering and ocean syphoning (Dutton & Lambeck, 2012; O’Leary et al., 2013;
 291 Figure 5). In contrast, RSL would rise throughout the LIG in the Bahamas due to the ongoing
 292 collapse of the peripheral bulge of the Laurentide Ice Sheet (Potter & Lambeck, 2004; Fig. 5).
 293 Proximity to the Laurentide Ice Sheet also governs the spatial pattern of RSL within the

294 Bahamas; the north-south gradient in Figure 1b reflects the difference in the level of isostatic
 295 equilibrium at 125 ka across the bulge relative to the present day (Potter and Lambeck, 2004;
 296 Creveling et al., 2017; Dyer et al., 2021). In contrast, RSL in western Australia (Figure 1c) does
 297 not show a significant gradient between sites because GIA across the coastline reflects an ocean
 298 loading signal that is roughly shoreline-parallel (Nakada & Lambeck, 1989; O’Leary et al.,
 299 2013). Differences between coral elevation distributions in the two regions (Figure 4) may in
 300 part be explained by differences in their RSL history (Figure 5).



301
 302 **Figure 5.** Relative sea level in the Bahamas and western Australia. (a) Relative sea level in the Bahamas
 303 (solid pink; Abaco Island) and western Australia (solid grey; Houtman Abrolhos Islands) for a single
 304 global mean sea level (GMSL; dashed black line) history during the Holocene (8 ka to present). (b) Same
 305 as a, but for the LIG, in the case of a stable sea level highstand of +5 m from 125-120 ka. GMSL history
 306 is identical to that shown in Fig. 1d.

307 3.2 Modeling preserved coral elevations at a single site

308 We begin with a case study to explore coral growth and preservation at two sites, Abaco
 309 Island in the Bahamas (star, Fig. 1b) and Houtman Abrolhos Islands in western Australia (star,

310 Fig. 1c). At each location, we force our coral model with RSL associated with two different
311 GMSL curves. The GMSL histories have the same highstand (~9 m) and peak type (ascending
312 peak), but different timing (early, Fig. 6a,c,e; and intermediate, Fig. 6b,d,f) and different
313 magnitudes of initial peaks (higher first peak in Figure 6a,c,e; lower initial peak in Figure 6b,d,f).
314 Hereafter, the GMSL histories are referred to as “early peak timing GMSL” and “intermediate
315 peak timing GMSL”. For each simulation, our model produces a present-day coral elevation
316 (Fig. 6a-d, red dot), which can be corrected to reflect LIG sea level (Fig. 6a-d, blue dot). The
317 modeled elevation at present day is the elevation one would expect the top of the LIG reef to be
318 observed today if it had experienced the modeled history of growth and erosion. The difference
319 in coral elevation in Figure 6b between the top of the reef at 112 ka and the present-day reflects
320 subsequent erosion of the reef during MIS 5a-d.

321 We compare modeled coral elevations using two RSL histories generated by the early
322 peak timing GMSL (Fig. 6a) and intermediate peak timing GMSL (Fig. 6d). In our model, coral
323 growth occurs when corals are below the sea surface and the rate of coral accretion exceeds the
324 rate of sea-level change (e.g., Fig. 6b,c,e,f). Coral erosion occurs when (1) sea level falls (e.g.,
325 Fig 6b,c,e,f) (2) corals are in the surf zone during a period of rapid sea-level rise that outpaces
326 the maximum rate of coral accretion and corals cannot keep up (e.g., Fig. 6b,e,f); or (3) when
327 post-LIG sea level is high enough to erode LIG corals (e.g., Fig. 6e). Coral elevation is static
328 when (1) the rate of sea-level rise exceeds the coral growth rate and thus corals cannot grow, but
329 corals are not in the surf zone and thus cannot be eroded (e.g., Fig. 6b,e,f); (2) corals have caught
330 up with sea level and can no longer grow towards the sea surface; or (3) corals are subaerially
331 exposed, but are not in the surf zone and thus cannot be eroded (e.g., Fig 6b,c,e,f). On Fig. 6,

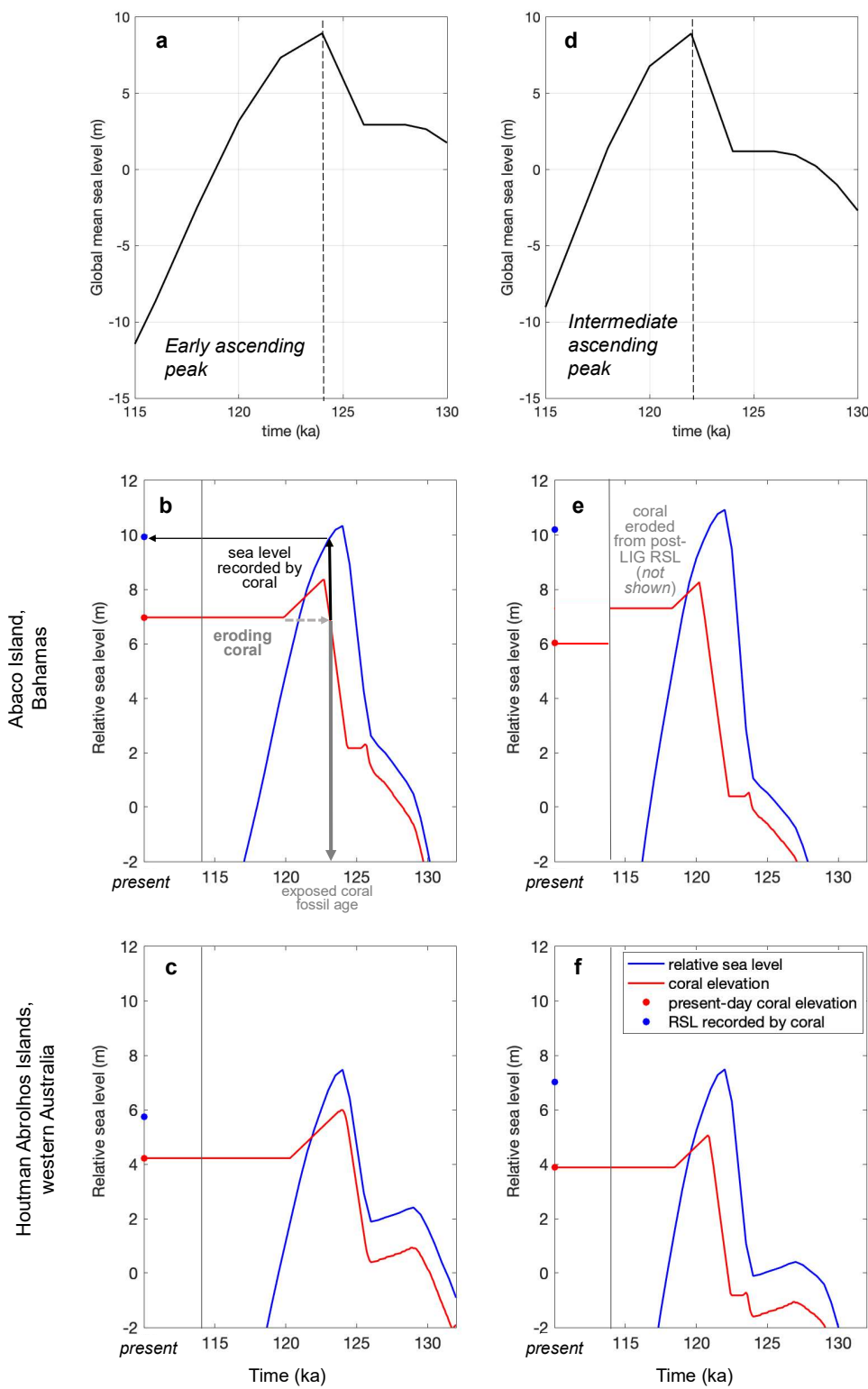
332 periods of coral erosion are shaded in grey, periods of coral growth are shaded in yellow, and
333 periods of static coral elevation are unshaded.

334 The results show that RSL histories with similar GMSL highstands can produce modeled
335 coral fossils with >1 m difference in present-day elevation due to GIA and the dynamic coral
336 response to sea-level change (growth effect). In the Bahamas (Fig. 6b,e), the two GMSL histories
337 produce RSL peaks that differ by 0.6 m (10.3 m in Fig. 6b; 10.9 m in Fig. 6e). However, the
338 preserved coral fossils both record RSL of ~10 m (9.9 m in Fig. 6b, 10.2 m in Fig. 6e). Thus, the
339 RSL peak is better captured by the coral experiencing the early ascending peak GMSL (Fig. 6b)
340 compared with the coral experiencing the intermediate ascending peak GMSL (Fig. 6e). This
341 effect is largely due to differences in post-LIG RSL; in the intermediate ascending peak GMSL,
342 subsequent erosion of LIG corals produces a large growth effect (Fig. 6e). We also note that
343 while the present-day coral elevations differ by ~1 m (7.0 m in Fig. 6b; 6.0 m in Fig. 6e), both
344 corals record the same magnitude of RSL, suggesting that different present-day coral elevations
345 are not necessarily indicative of different recorded sea levels.

346 In western Australia, at Houtman Abrolhos Islands (Fig. 6c,f), the RSL peaks are
347 equivalent (7.5 m) across the two GMSL histories. This RSL peak is well-captured by the coral
348 experiencing the intermediate ascending peak GMSL (Fig. 6f; RSL recorded by the coral is 7.0
349 m), but is not well-captured by the coral experiencing the early ascending peak GMSL (Fig. 6c;
350 RSL recorded by the coral is 5.7 m). With the early ascending peak GMSL, RSL falls more
351 gradually after the peak GMSL, leading to a longer period of coral erosion and a lower present-
352 day coral elevation. This indicates that even when no post-LIG erosion occurs, the same RSL
353 peak can produce different present-day coral elevations depending on rates of LIG sea-level
354 change. Thus, the growth effect has the potential to introduce additional uncertainty into sea-

355 level reconstructions since the corrections to reconstruct LIG sea level using our process-based
356 coral model depend on the GMSL histories.

ORIGINAL UNEDITED MANUSCRIPT



358 **Figure 6.** Evolution of reef growth in response to sea level. (a) GMSL history with an early
 359 ascending Last Interglacial (LIG) peak, corresponding to RSL curves in b-c. Timing of the
 360 GMSL highstand is indicated with a dashed black line. (b) Relative sea level history (RSL; blue

line) at Abaco Island (starred location in Figure 1b), Bahamas produced by the GMSL in (a). Coral elevation (top of the modeled coral reef) as a function of RSL is shown with a red line. On the left axis, the present-day coral elevation is shown as a red dot, and the RSL recorded by the present-day coral (RSL at the time when the top of the reef was formed) is shown as a blue dot. A schematic for calculating the RSL recorded by the present-day coral is shown, with the age of the exposed coral fossil marked in dark grey on the x-axis (time axis). Shading indicates whether the coral is catching up to sea level (yellow) or eroding (grey). Coral elevation is static where there is no shading. (c) Same as b, for RSL at Houtman Abrolhos Islands (starred location in Figure 1c), western Australia. (d-f) Same as a-c, for a GMSL history with an intermediate ascending LIG peak.

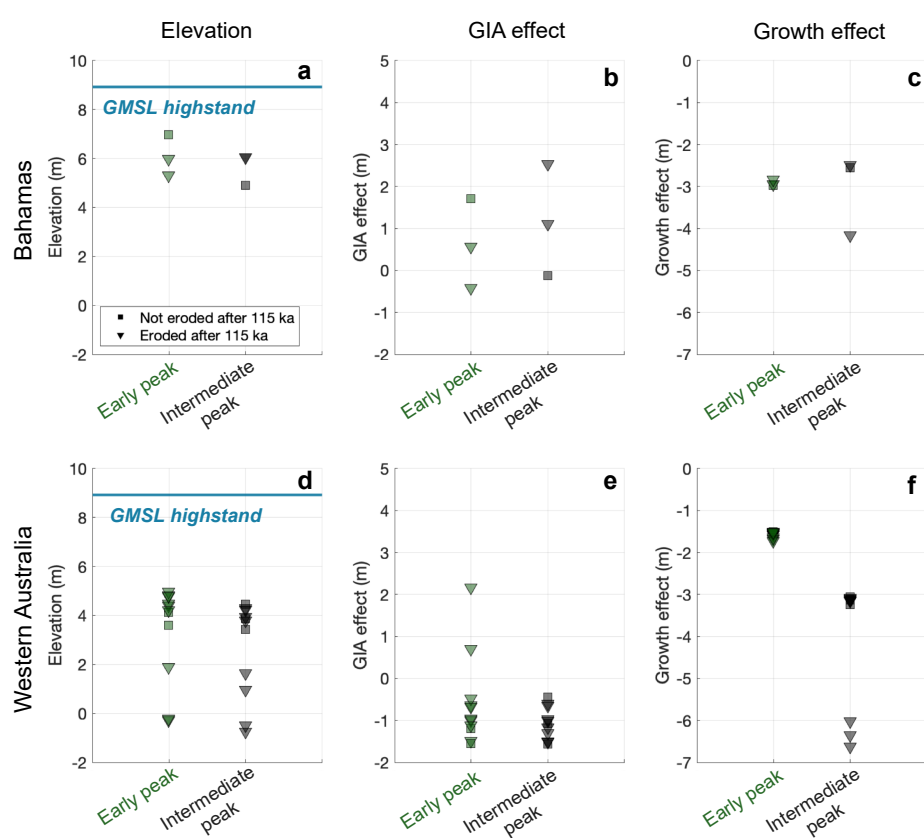
371 3.3 Modeling preserved coral elevations across sites

372 The magnitude of the growth effect (i.e. the difference between blue and red dot in Fig. 373 6b,c,e,f) varies with location, and differs between the near-field (Bahamas) and the far-field 374 (western Australia). We next examine simulated coral elevations across the Bahamas and 375 western Australia produced by the same two GMSL histories. The early ascending peak GMSL 376 (Fig. 6a) and intermediate ascending peak GMSL (Fig. 6b) produce distinct predicted LIG coral 377 elevations, GIA effects, and growth effects across all sites in the Bahamas (Figure 7a-c) and 378 western Australia (Figure 7d-f).

379 In the Bahamas, coral elevations in the Bahamas simulated by intermediate ascending 380 peak GMSL are lower than those simulated by the early ascending peak GMSL because the 381 intermediate ascending peak GMSL has higher sea level during MIS 5a-d, leading to post-LIG 382 erosion of some LIG corals (corals that eroded after LIG are indicated by triangles on Fig. 7a). 383 Generally, corals that eroded after the LIG have lower elevations, although this is not always the 384 case (e.g., green squares in Fig. 7a). The growth effect varies across sites (e.g., Figure 7c), most 385 notably due to erosion; corals that experienced post-LIG erosion are associated with significantly 386 larger-magnitude growth effects. This demonstrates that gradients of coral elevations across sites 387 – which have been assumed to be representative of GIA gradients (e.g., Potter and Lambeck, 388 2004) – can be produced by an interplay of GIA and coral growth and erosion, although we note

389 that on large spatial scales the GIA effect will dominate the growth effect. This is particularly
 390 important to consider when coral elevations are interpreted without consideration (or
 391 elimination) of corals that show erosion.

392 In western Australia, the growth effect varies more dramatically within a single
 393 simulation (~4.5 m range in growth effect when forced with the intermediate ascending peak
 394 GMSL). As in the Bahamas, the corals that experienced post-LIG erosion are associated with
 395 significantly larger-magnitude growth effects (Fig. 7f). We also note that the growth effect
 396 across the two GMSL histories varies more widely in western Australia due to more significant
 397 post-LIG erosion at some sites when the corals are forced with the intermediate ascending peak
 398 GMSL.



399
 400 **Figure 7.** Present-day modeled coral fossil elevation distributions and associated GIA and
 401 growth effects. (a) Present-day modeled coral elevations at all sites in the Bahamas produced by

402 two GMSL histories (early ascending GMSL peak, Fig. 6a; intermediate ascending GMSL peak,
403 Fig. 6b). GMSL highstands (~ 9 m) are shown with horizontal blue lines. Corals that experienced
404 post-LIG erosion (erosion after 115 ka) are indicated with triangles. (b) GIA effect (eustatic sea
405 level subtracted from RSL at time of coral death) of present-day modeled corals forced by two
406 GMSL histories. (c) Same as b, for the coral growth effect (RSL at time of coral death subtracted
407 from present-day coral elevation). (d-f) Same as a-c, for western Australia.

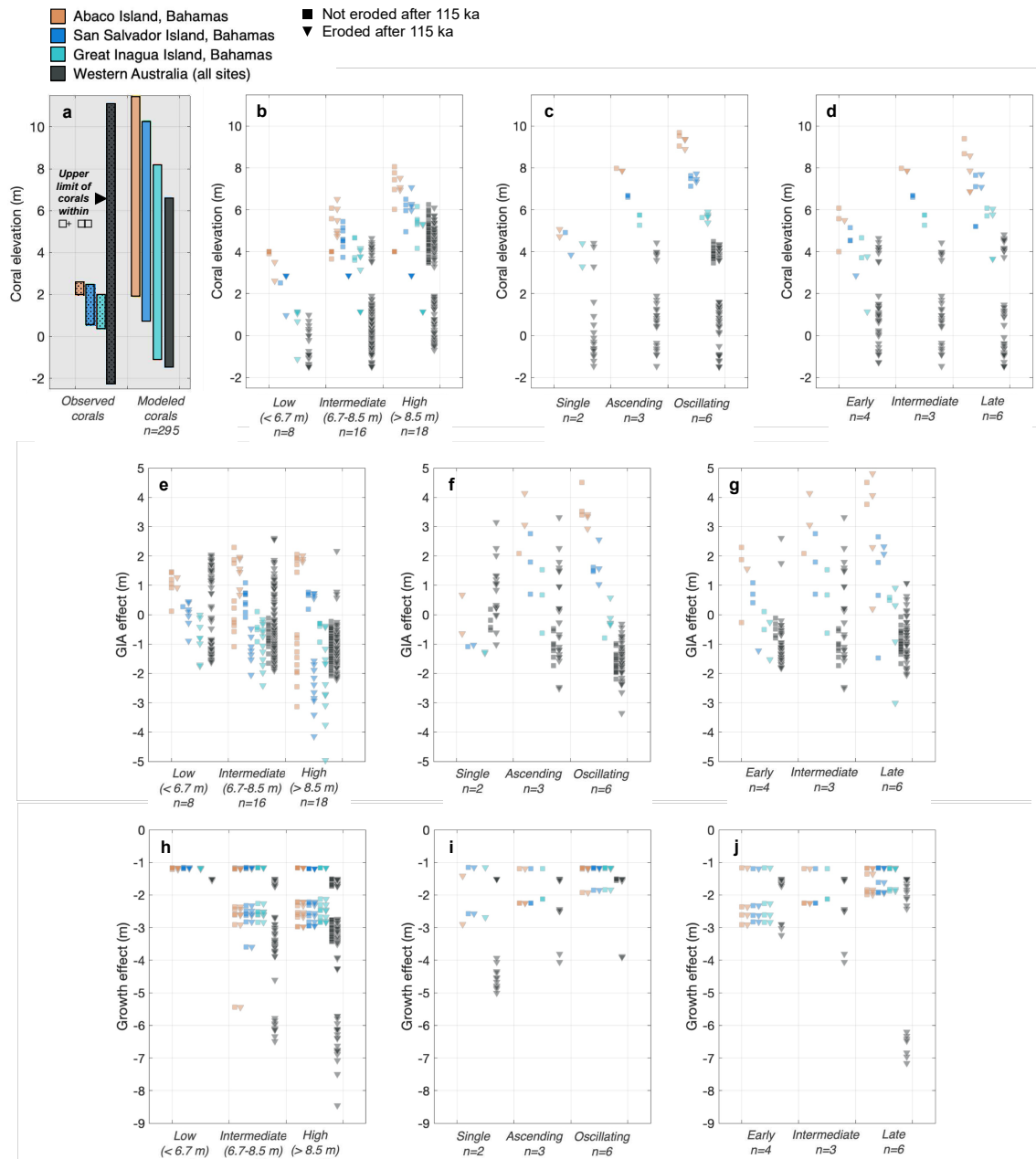
408 **3.4 Modeled coral elevation distributions using a range of LIG global ice volume histories**

409 Next, we force our coral model at each LIG coral site with the relative sea-level histories
410 associated with the 900 GMSL histories (Fig. 2). To extract LIG corals from our simulation, we
411 filter for reefs with exposed surfaces last growing between 132-115 ka. Of 900 simulations, 295
412 produce modeled LIG reefs at all sites in the Bahamas and 11 of the 15 sites in western Australia
413 where observed LIG corals exist. The ranges of modeled coral elevations produced across all
414 these runs at each site in the Bahamas and across western Australia are shown in Figure 8a (solid
415 bars). Ranges of observed coral elevations are shown for comparison (Fig. 8a, dotted bars).

416 We examine how different GMSL histories produce different modeled coral
417 elevations. We present subsets of the full 295 simulations in Fig. 8b-d to isolate the impacts of
418 LIG peak timing, peak magnitude, and peak type on the modeled coral elevations. To begin, we
419 consider modeled corals produced by a range of highstand values, controlling for type of GMSL
420 peak and timing (ascending GMSL peaks and early GMSL peak timing; Figure 8b). As the
421 highstand value increases, the upper bounds on the coral elevation ranges increase at all sites.
422 We next consider how modeled coral elevation varies with peak type (Figure 8c) and timing
423 (Figure 8d) by holding the GMSL highstand constant at ~ 7.8 m. The range of modeled coral
424 elevations in western Australia is similar across these subsets (Figure 8; blue). However, the
425 range of modeled coral elevations in the Bahamas is highly sensitive to variations in peak type
426 and peak timing; single peaks and early peaks produce a lower range of modeled coral elevations

427 at all three Bahamian sites than ascending or oscillating GMSL peaks or GMSL peaks with
 428 intermediate or late timing (Figure 8b-d).

429



430

431 **Figure 8.** Present-day modeled coral fossil elevations produced after forcing the coral model with GMSL
 432 histories, and associated GIA and growth effects. (a) Range of coral elevations at each Bahamian site

433 (Abaco Island, pink; San Salvador, blue; Great Inagua, teal) and across all sites in western Australia
434 (grey), for observed (dotted) and modeled (solid) corals across all GMSL histories. For western Australia,
435 we mark the upper elevation range of corals within 2 standard deviations of the mean. (b-d) Present-day
436 modeled coral fossil elevations after forcing the coral model with subsets of GMSL histories. We note the
437 number (n) of GMSL histories represented, i.e. those that produce corals dating to the LIG at sites
438 included in the Hibbert database (Hibbert et al., 2016), in each subset. Individual corals are indicated with
439 squares (not eroded after 115 ka) and triangles (eroded after 115 ka). In (b), peak type and timing are held
440 constant while only varying the GMSL highstand. In (c), peak timing and GMSL highstand are held
441 constant while only varying the type, and in (d) peak type and GMSL highstand are held constant while
442 only varying the peak timing. (e-g) Same as b-d, for GIA effects of modeled corals (eustatic sea level
443 subtracted from RSL at time of coral death). (h-j) Same as b-d, for the coral growth effect (RSL at time
444 of coral death subtracted from present-day coral elevation).

445 **3.5 Comparing the impact of glacial isostatic adjustment (GIA) and coral dynamics**

446 Different model runs produce different magnitudes of the growth effect (growth effect
447 varies between ~ -8.5 m to tidal depth; Fig. 8h-j). A wider range of the growth effect implies
448 more uncertainty in the depth at which corals at that site grew below the sea surface. Because the
449 growth effect is not constant across runs, even after controlling for peak type, peak magnitude,
450 and/or peak timing, RSL reconstructions that rely on coral fossils may be subject to additional
451 uncertainty resulting from an unknown growth effect. For example, if a growth effect of tidal
452 depth is assumed to be constant across sites (implying that corals were fully caught up to RSL
453 when they died), reconstructions could underestimate RSL by up to ~ 7 m. The growth effect (and
454 thus the potential to underestimate RSL) tends to be higher in magnitude for corals that
455 experienced post-LIG erosion (triangles, Fig. 8h-j); however, even for corals that did not

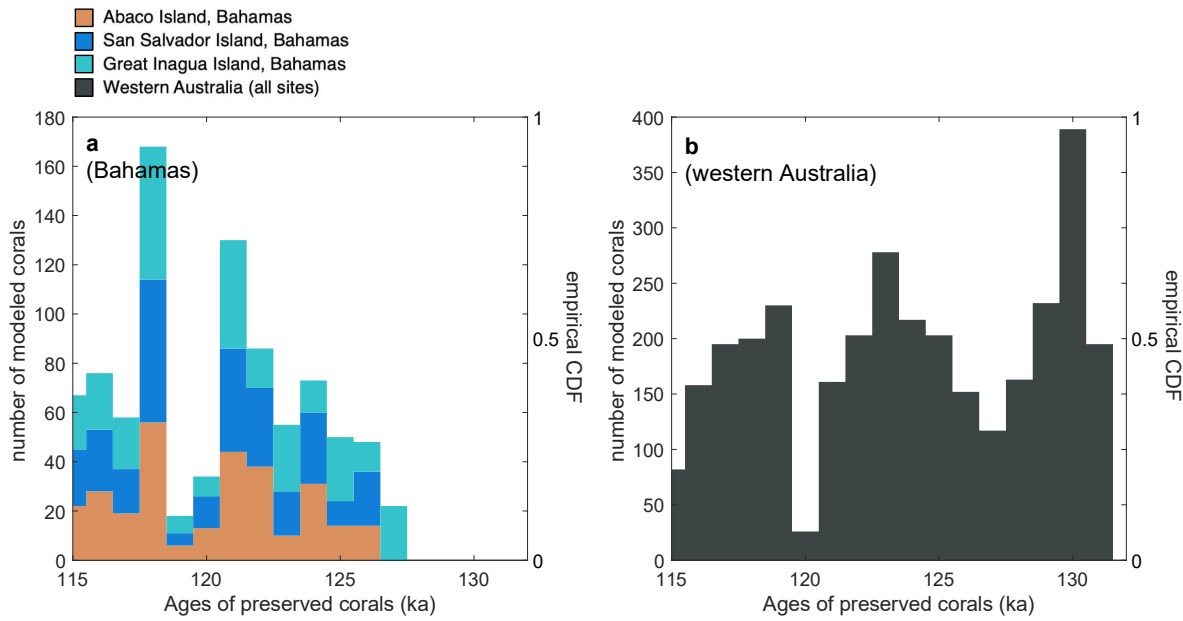
456 experience post-LIG erosion (squares, Fig. 8h-j), reconstructions could underestimate RSL by up
457 to ~4.5 m.

458 In our model, higher-magnitude GMSL peaks increase the upper bound on coral
459 elevations; as GMSL highstands increase, corals respond by growing to higher elevations. More
460 prolonged peaks (ascending or oscillating GMSL peaks) increase the upper and lower limits of
461 coral elevation at every site in the Bahamas, allowing more time for the corals to catch up to sea
462 level than the shorter single peaks. The modeled elevation range at the Bahamas is sensitive to
463 relative sea-level gradients along the peripheral bulge of the North American ice sheet (Figure
464 1b), illustrated by the differences in the GIA effect across Abaco Island, San Salvador Island,
465 and Great Inagua Island (Fig 8e-g). GIA has a ~ -5 to +5 m effect on modeled coral elevations in
466 the Bahamas (Figure 8e-g). The growth effect is mostly ~ -3 m to tidal depth (-1.15 m) in the
467 Bahamas, with a wider spread of growth effect values at the northernmost site (Abaco Island,
468 down to -5.5 m) due to its location on the peripheral bulge. Abaco Island is characterized by the
469 highest GIA-induced sea-level rise, and the reefs struggle to keep up with the more rapid sea-
470 level rise.

471 Because LIG RSL in western Australia is characterized by an early peak followed by a
472 relative sea-level fall (Figure 5), corals are more likely to keep up with sea level with a slower
473 deglaciation (and later GMSL peak timing). The GIA effect here varies between ~ -3 to +3 m.
474 For each GMSL subset, the range of the GIA effect across western Australia is wider than the
475 range of the GIA effect across the Bahamas, despite the larger GIA gradient across sites in the
476 Bahamas (Fig. 1b cf. Fig. 1c). This feature is due to post-LIG erosion in western Australia. There
477 is wider age distribution in western Australia because Holocene RSL rose above present-day sea
478 level (Figure 5), which erodes the most-recent coral, and creates LIG coral surfaces with older

479 ages than in the Bahamas (Figure 9). The corals in western Australia sample RSL across a
480 greater duration of the LIG, and are thus characterized by a wider range of GIA corrections.

481 This simulated Holocene erosion also results in the wider range of the growth effect
482 magnitude in western Australia, since corals can be eroded to older ages when the reef had not
483 yet caught up to sea level. These results indicate that the growth effect varies with the cumulative
484 history of GIA effects, and is sensitive to both RSL during the LIG and subsequent highstands
485 which may have eroded the preserved corals.



486
 487 **Figure 9.** Modeled age distribution for corals in the Bahamas and western Australia. Ages of preserved
 488 LIG corals in the Bahamas (a) and western Australia (b). Modeled corals are only included from the 295
 489 simulations which produced modeled LIG reefs at all sites in the Bahamas and 11 of the 15 sites in
 490 western Australia where observed LIG corals exist. Colors correspond to coral site (Abaco Island, pink;
 491 San Salvador, blue; Great Inagua, teal; western Australia, grey). Empirical cumulative distribution
 492 function (CDF) of all corals in each region is shown in solid grey, with a corresponding y-axis on the
 493 right.

494

495 While the upper bound on modeled coral elevation range in western Australia is
 496 substantially lower than the observed coral elevation range (11.1 m for the observed range and
 497 6.7 for the modeled range), only 9 out of 102 samples in the dataset of observed elevations are
 498 >6.6 m, and these fall more than two standard deviations away from the mean. Five of the nine
 499 samples are located at Cape Cuvier and Cape Range, where several prior studies have argued
 500 there to be Quaternary tectonic activity (e.g., D. Clark, 2010; Condon et al., 1955; Sandstrom et
 501 al., 2020; Whitney & Hengesh, 2015). If we remove elevation data in western Australia that fall

502 more than 2 standard deviations away from the mean, the upper bound on the range of observed
503 coral fossil elevations is 6.6 m, similar to the modeled range (black triangle; Figure 8A). There
504 are also two locations (San Salvador Island and Vlaming Head in western Australia) where the
505 lower bound on observed coral elevations does not overlap with the range of modeled coral
506 elevations. This may be due to our assumption that corals are caught up with sea level at the time
507 of their initialization.

508 None of the simulations produce LIG reefs at 4 of the sites in western Australia (Burney
509 Point, 2 sites at Shark Bay, and Leander Point), where 19 coral fossil data points are observed.
510 This is likely due to erosion of coral fossils in our model during the higher Holocene RSL in
511 western Australia. Erosion is a testable feature in our model; for example, past studies have
512 suggested that Shark Bay coral communities have high potential for ongoing erosion (O’Leary et
513 al., 2008). Because of the simplifying assumptions we make in constructing our coral model, our
514 modeled coral results should not be quantitatively compared with observations. However,
515 locations of post-LIG coral erosion in our model can be tuned to locations of eroded corals in the
516 observational record, which would allow for a qualitative comparison between our coral model
517 results and field observations.

518 **3.6 Modeling limitations**

519 To isolate the impacts of GMSL on coral growth and erosion, our study makes a set of
520 simplifying assumptions. Firstly, our coral model uses constant maximum accretion and erosion
521 rates, although these values are unlikely to be the same across coral species. Our model also does
522 not include lateral accretion or allow for different wave regimes depending on local topography,
523 which would influence reef growth and preservation (Woodroffe & Webster, 2014). An example
524 of a more complex reef evolution model which includes topographic and sediment effects can be

525 found in Salles et al. (2018). Including these effects would likely spread the elevation
526 distribution of modeled preserved coral fossils, and potentially would allow for direct
527 comparisons between modeled coral fossil elevations and observed coral fossil elevations.

528 Secondly, our GIA simulations adopt a single ice distribution configuration and a single
529 Earth model for each region. Varying the region and timing of excess ice melt during the LIG,
530 including generating ice histories with different ice geometries, would impact the shape of
531 modeled coral distributions given the sensitivity of our coral model to RSL changes over the
532 LIG. For example, a collapse of the West Antarctic Ice Sheet at different times during the LIG
533 would influence RSL histories in western Australia and the Bahamas, and these would produce
534 distinctive modeled coral distributions (Hay et al., 2014). In addition to being sensitive to the
535 melt source during the LIG, these results are also sensitive to the ice distribution prior to the
536 LIG. RSL at the Bahamas, and therefore the distribution of coral elevation at the Bahamas, is
537 highly sensitive to the size of the MIS 6 Laurentide ice sheet and its speed of deglaciation
538 (Dendy et al., 2017). Accounting for different temporal and spatial patterns of ice sheet melt
539 across the LIG on coral elevation distributions, in addition to different viscoelastic Earth
540 structures, should be the subject of future study.

541

542

543 **5 CONCLUSIONS**

544 By modeling coral growth and erosion in response to sea-level change, we demonstrated
545 that the elevations of preserved LIG corals in the near- and far-field are sensitive to the
546 magnitude, rate, and timing of global mean sea-level change over the LIG. In particular, we

547 performed a suite of GIA simulations spanning a wide range of possible LIG sea-level histories
548 and simulated the evolution of LIG corals in response to the relative sea-level change in the
549 Bahamas and western Australia. This allowed us to systematically isolate the influence of GIA
550 on modeled coral elevations, which is distinct from the influence of dynamic coral growth and
551 erosion.

552 Although this work makes a series of simplifying assumptions, our findings illustrate that
553 coral growth and erosion in response to local sea-level change influences the coral's preserved
554 age, present-day elevation, and depth below the sea-surface at its time of most recent growth
555 (which we call the growth effect). Across our simulations, the growth effect has a maximum
556 magnitude of 5.4 m in corals that did not experience post-LIG erosion and can be even larger
557 (8.9 m) in corals that did experience post-LIG erosion, although the mean growth effect is
558 significantly smaller (approximately 1.6 m in the Bahamas and 2 m in western Australia, for both
559 eroded and non-eroded corals). The dynamic response of coral growth to sea-level change
560 introduces uncertainty into RSL reconstructions, with the magnitude of this uncertainty
561 dependent on chosen parameter values, location, and sea-level history.

562 To constrain the true magnitude of the growth effect, future work could invoke an inverse
563 coral model to reconstruct RSL using the present-day distribution of LIG corals. Field
564 observations of post-LIG coral erosion could also inform estimates of the growth effect. In
565 addition, an improved coral model which incorporates more complex processes, including
566 species-specific growth and erosion patterns and lateral accretion, may be used to explore a
567 range of GMSL scenarios and melt patterns, producing modeled elevation distributions which
568 can be compared to observed elevation distributions in both the Bahamas and western Australia.
569 Such exercises could demonstrate the potential of coral modeling as an innovative tool to reduce

570 uncertainty in coral-based LIG RSL reconstructions, given that only certain GMSL histories will
571 produce good fits between the observed and modeled elevations. One advantage to such an
572 approach is that comparing modeled and observed coral elevation distributions does not require
573 good age control beyond an association with the LIG. While corals tend to have good age
574 constraints, they can be plagued by open-system behavior. Furthermore, other LIG sea-level
575 indicators such as marine terraces and erosional notches have significantly larger age
576 uncertainties and applying a similar process-based approach may also provide new insight from
577 these datasets.

578

579 **ACKNOWLEDGEMENTS**

580 JA acknowledges support from NSF award MGG 18-41888. Funding was provided by Harvard
581 University and NSF grant OCE-1702684 (JXM). TP acknowledges support from Harvard
582 University, NSF EAR Postdoctoral Fellowship and UC President's Postdoc Program Fellowship.
583 RCS, TP, JXM, JA, and PJH designed the study and wrote the manuscript. RCS performed the
584 modeling and analysis. We thank the editor, Yucheng Lin, and an anonymous reviewer for their
585 comments and improvements to the manuscript.

586

587

588 **DATA AVAILABILITY STATEMENT**

589 The Last Interglacial coral fossil elevation database used in this study (see Figures 1, 4) is
 590 archived by British Oceanographic Data Centre (BODC; www.bodc.ac.uk) doi:
 591 10.5285/32056c4c-fef8-29c4-e053-6c86abc06cd4 (Hibbert et al., 2016). Global mean sea level
 592 histories used in this study and a MATLAB version of the coral model will be made available at
 593 https://github/becca-cs/lig_coral prior to publication.

594

595

596 **REFERENCES**

- 597 Barlow, N. L. M., McClymont, E. L., Whitehouse, P. L., Stokes, C. R., Jamieson, S. S. R.,
 598 Woodroffe, S. A., Bentley, M. J., Callard, S. L., Cofaigh, C. Ó., Evans, D. J. A., Horrocks, J. R.,
 599 Lloyd, J. M., Long, A. J., Margold, M., Roberts, D. H., & Sanchez-Montes, M. L. (2018). Lack
 600 of evidence for a substantial sea-level fluctuation within the Last Interglacial. *Nature
 Geoscience*, 11(9), 627–634. <https://doi.org/10.1038/s41561-018-0195-4>
 601 Blanchon, P., Eisenhauer, A., Fietzke, J., & Liebetrau, V. (2009). Rapid sea-level rise and reef
 602 back-stepping at the close of the last interglacial highstand. *Nature*, 458(7240), 881–884.
 603 <https://doi.org/10.1038/nature07933>
 604 Bosscher, H., & Schlager, W. (1992). Computer simulation of reef growth. *Sedimentology*, 39,
 605 503–512. <https://doi.org/10.1111/j.1365-3091.1992.tb02130.x>
 606 Boyden, P., Stocchi, P., & Rovere, A. (2023). *Refining patterns of melt with forward
 607 stratigraphic models on stable Pleistocene coastlines* [Preprint]. Physical: Landscape Evolution:
 608 modelling and field studies. <https://doi.org/10.5194/egusphere-2023-95>
 609 Chutcharavan, P. M., & Dutton, A. (2021). A global compilation of U-series-dated fossil coral
 610 sea-level indicators for the Last Interglacial period (Marine Isotope Stage 5e). *Earth System
 611 Science Data*, 13(7), 3155–3178. <https://doi.org/10.5194/essd-13-3155-2021>
 612 Clark, D. (2010). Identification of Quaternary scarps in southwest and central west Western
 613 Australia using DEM-based hill shading: Application to seismic hazard assessment and
 614 neotectonics. *International Journal of Remote Sensing*, 31(23), 6297–6325.
 615 Clark, P. U., He, F., Golledge, N. R., Mitrovica, J. X., Dutton, A., Hoffman, J. S., & Dendy, S.
 616 (2020). Oceanic forcing of penultimate deglacial and last interglacial sea-level rise. *Nature*,
 617 577(7792), 660–664. <https://doi.org/10.1038/s41586-020-1931-7>
 618 Colleoni, F., Wekerle, C., Näslund, J.-O., Brandefelt, J., & Masina, S. (2016). Constraint on the
 619 penultimate glacial maximum Northern Hemisphere ice topography (\approx 140 kyrs BP). *Quaternary
 620 Science Reviews*, 137, 97–112. <https://doi.org/10.1016/j.quascirev.2016.01.024>

- 622 Condon, M. A., Johnstone, D., & Perry, W. J. (1955). The Cape Range structure Western
 623 Australia. *Commonwealth of Australia Department of National Development Bureau of Mineral
 624 Resources Geology and Geophysics Bulletin*, 21, 107.
- 625 Creveling, J. R., Mitrovica, J. X., Clark, P. U., Waelbroeck, C., & Pico, T. (2017). Predicted
 626 bounds on peak global mean sea level during marine isotope stages 5a and 5c. *Quaternary
 627 Science Reviews*, 163, 193–208. <https://doi.org/10.1016/j.quascirev.2017.03.003>
- 628 Cutler, K. B., Edwards, R. L., Taylor, F. W., Cheng, H., Adkins, J., Gallup, C. D., Cutler, P. M.,
 629 Burr, G. S., & Bloom, A. L. (2003). Rapid sea-level fall and deep-ocean temperature change
 630 since the last interglacial period. *Earth and Planetary Science Letters*, 206(3–4), 253–271.
 631 [https://doi.org/10.1016/S0012-821X\(02\)01107-X](https://doi.org/10.1016/S0012-821X(02)01107-X)
- 632 Dalton, A. S., Stokes, C. R., & Batchelor, C. L. (2022). Evolution of the Laurentide and Innuitian
 633 ice sheets prior to the Last Glacial Maximum (115 ka to 25 ka). *Earth-Science Reviews*, 224,
 634 103875. <https://doi.org/10.1016/j.earscirev.2021.103875>
- 635 de Gelder, G., Husson, L., Pastier, A.-M., Fernández-Blanco, D., Pico, T., Chauveau, D.,
 636 Authemayou, C., & Pedoja, K. (2022). High interstadial sea levels over the past 420ka from the
 637 Huon Peninsula, Papua New Guinea. *Communications Earth & Environment*, 3(1), 256.
 638 <https://doi.org/10.1038/s43247-022-00583-7>
- 639 Dechnik, B., Webster, J. M., Webb, G. E., Nothdurft, L., Dutton, A., Braga, J.-C., Zhao, J.,
 640 Duce, S., & Sadler, J. (2017). The evolution of the Great Barrier Reef during the Last Interglacial
 641 Period. *Global and Planetary Change*, 149, 53–71.
 642 <https://doi.org/10.1016/j.gloplacha.2016.11.018>
- 643 DeConto, R. M., Pollard, D., Alley, R. B., Velicogna, I., Gasson, E., Gomez, N., Sadai, S.,
 644 Condron, A., Gilford, D. M., Ashe, E. L., Kopp, R. E., Li, D., & Dutton, A. (2021). The Paris
 645 Climate Agreement and future sea-level rise from Antarctica. *Nature*, 593(7857), 83–89.
 646 <https://doi.org/10.1038/s41586-021-03427-0>
- 647 Dendy, S., Austermann, J., Creveling, J. R., & Mitrovica, J. X. (2017). Sensitivity of Last
 648 Interglacial sea-level high stands to ice sheet configuration during Marine Isotope Stage 6.
 649 *Quaternary Science Reviews*, 171, 234–244. <https://doi.org/10.1016/j.quascirev.2017.06.013>
- 650 Dutton, A., & Lambeck, K. (2012). Ice Volume and Sea Level During the Last Interglacial.
 651 *Science*, 337(6091), 216–219. <https://doi.org/10.1126/science.1205749>
- 652 Dyer, B., Austermann, J., D'Andrea, W. J., Creel, R. C., Sandstrom, M. R., Cashman, M.,
 653 Rovere, A., & Raymo, M. E. (2021). Sea-level trends across The Bahamas constrain peak last
 654 interglacial ice melt. *Proceedings of the National Academy of Sciences*, 118(33), e2026839118.
 655 <https://doi.org/10.1073/pnas.2026839118>
- 656 Hay, C., Mitrovica, J. X., Gomez, N., Creveling, J. R., Austermann, J., & E. Kopp, R. (2014).
 657 The sea-level fingerprints of ice-sheet collapse during interglacial periods. *Quaternary Science
 658 Reviews*, 87, 60–69. <https://doi.org/10.1016/j.quascirev.2013.12.022>
- 659 Hearn, C. J. (1999). Wave-breaking hydrodynamics within coral reef systems and the effect of
 660 changing relative sea level. *Journal of Geophysical Research: Oceans*, 104(C12), 30007–30019.
 661 <https://doi.org/10.1029/1999JC900262>
- 662 Hearty, P. J., Hollin, J. T., Neumann, A. C., O'Leary, M. J., & McCulloch, M. (2007). Global
 663 sea-level fluctuations during the Last Interglaciation (MIS 5e). *Quaternary Science Reviews*,
 664 26(17–18), 2090–2112. <https://doi.org/10.1016/j.quascirev.2007.06.019>
- 665 Hibbert, F. D., Rohling, E. J., Dutton, A., Williams, F. H., Chutcharavan, P. M., Zhao, C., &
 666 Tamisiea, M. E. (2016). Coral indicators of past sea-level change: A global repository of U-

- 667 series dated benchmarks. *Quaternary Science Reviews*, 145, 1–56.
 668 <https://doi.org/10.1016/j.quascirev.2016.04.019>
- 669 Hoffman, J., Clark, P. U., Parnell, A. C., & He, F. (2017). Regional and global sea-surface
 670 temperatures during the last interglaciation. *Science*, 355(6322), 276–279.
 671 <https://doi.org/10.1126/science.aai8464>
- 672 Hopley, D. (Ed.). (2011). *Encyclopedia of Modern Coral Reefs*. Springer Netherlands.
 673 <https://doi.org/10.1007/978-90-481-2639-2>
- 674 Kendall, R. A., Mitrovica, J. X., & Milne, G. A. (2005). On post-glacial sea level—II. Numerical
 675 formulation and comparative results on spherically symmetric models. *Geophysical Journal
 676 International*, 161(3), 679–706. <https://doi.org/10.1111/j.1365-246X.2005.02553.x>
- 677 Kleypas, J. A. (1997). Modeled estimates of global reef habitat and carbonate production since
 678 the Last Glacial Maximum. *Paleoceanography*, 12(4), 533–545.
 679 <https://doi.org/10.1029/97PA01134>
- 680 Kopp, R. E., Simons, F. J., Mitrovica, J. X., Maloof, A. C., & Oppenheimer, M. (2009).
 681 Probabilistic assessment of sea level during the last interglacial stage. *Nature*, 462(7275), 863–
 682 867. <https://doi.org/10.1038/nature08686>
- 683 Kopp, R. E., Simons, F. J., Mitrovica, J. X., Maloof, A. C., & Oppenheimer, M. (2013). A
 684 probabilistic assessment of sea level variations within the last interglacial stage. *Geophysical
 685 Journal International*, 193(2), 711–716. <https://doi.org/10.1093/gji/ggt029>
- 686 Milne, G. A., & Mitrovica, J. X. (1996). Postglacial sea-level change on a rotating Earth: First
 687 results from a gravitationally self-consistent sea-level equation. *Geophysical Journal
 688 International*, 126(3), F13–F20. <https://doi.org/10.1111/j.1365-246X.1996.tb04691.x>
- 689 Milne, G. A., & Mitrovica, J. X. (1998). Postglacial sea-level change on a rotating Earth.
 690 *Geophysical Journal International*, 133(1), 1–19. [246X.1998.1331455.x](https://doi.org/10.1046/j.1365-

 691 246X.1998.1331455.x)
- 692 Milne, G. A., Mitrovica, J. X., & Davis, J. L. (1999). *Near-field hydro-isostasy: The
 693 implementation of a revised sea-level equation*. 19.
- 694 Milne, G. A., & Peros, M. (2013). Data–model comparison of Holocene sea-level change in the
 695 circum-Caribbean region. *Global and Planetary Change*, 107, 119–131.
 696 <https://doi.org/10.1016/j.gloplacha.2013.04.014>
- 697 Nakada, M., & Lambeck, K. (1989). Late Pleistocene and Holocene sea-level change in the
 698 Australian region and mantle rheology. *Geophysical Journal International*, 96(3), 497–517.
 699 <https://doi.org/10.1111/j.1365-246X.1989.tb06010.x>
- 700 Neumann, A., & Hearty, P. J. (1996). Rapid sea-level changes at the close of the last interglacial
 701 (substage 5e) recorded in Bahamian island geology. *Geology*, 24(9), 775.
 702 [https://doi.org/10.1130/0091-7613\(1996\)024<0775:RSLCAT>2.3.CO;2](https://doi.org/10.1130/0091-7613(1996)024<0775:RSLCAT>2.3.CO;2)
- 703 Neumann, A., & Macintyre, I. (1985). Reef response to sea level rise: Keep-up, catch-up or give
 704 up. *Proceedings of the Fifth International Coral Reef Congress*, 3, 105–110.
- 705 O’Leary, M. J., Hearty, P. J., & McCulloch, M. T. (2008). U-series evidence for widespread reef
 706 development in Shark Bay during the last interglacial. *Palaeogeography, Palaeoclimatology,
 707 Palaeoecology*, 259(4), 424–435. <https://doi.org/10.1016/j.palaeo.2007.10.022>
- 708 O’Leary, M. J., Hearty, P. J., Thompson, W. G., Raymo, M. E., Mitrovica, J. X., & Webster, J.
 709 M. (2013). Ice sheet collapse following a prolonged period of stable sea level during the last
 710 interglacial. *Nature Geoscience*, 6(9), 796–800. <https://doi.org/10.1038/ngeo1890>
- 711 Pastier, A. -M., Husson, L., Pedoja, K., Bézos, A., Authemayou, C., Arias-Ruiz, C., & Cahyarini,
 712 S. Y. (2019). Genesis and Architecture of Sequences of Quaternary Coral Reef Terraces: Insights

- 713 From Numerical Models. *Geochemistry, Geophysics, Geosystems*, 20(8), 4248–4272.
714 <https://doi.org/10.1029/2019GC008239>
- 715 Peltier, W. R. (2004). GLOBAL GLACIAL ISOSTASY AND THE SURFACE OF THE ICE-
716 AGE EARTH: The ICE-5G (VM2) Model and GRACE. *Annual Review of Earth and Planetary
717 Sciences*, 32(1), 111–149. <https://doi.org/10.1146/annurev.earth.32.082503.144359>
- 718 Pico, T., Mitrovica, J. X., Ferrier, K. L., & Braun, J. (2016). Global ice volume during MIS 3
719 inferred from a sea-level analysis of sedimentary core records in the Yellow River Delta.
720 *Quaternary Science Reviews*, 152, 72–79. <https://doi.org/10.1016/j.quascirev.2016.09.012>
- 721 Potter, E.-K., & Lambeck, K. (2004). Reconciliation of sea-level observations in the Western
722 North Atlantic during the last glacial cycle. *Earth and Planetary Science Letters*, 217(1–2), 171–
723 181. [https://doi.org/10.1016/S0012-821X\(03\)00587-9](https://doi.org/10.1016/S0012-821X(03)00587-9)
- 724 Rohling, E. J., Grant, K., Hemleben, Ch., Siddall, M., Hoogakker, B. A. A., Bolshaw, M., &
725 Kucera, M. (2008). High rates of sea-level rise during the last interglacial period. *Nature
726 Geoscience*, 1(1), 38–42. <https://doi.org/10.1038/ngeo.2007.28>
- 727 Rohling, E. J., Hibbert, F. D., Williams, F. H., Grant, K. M., Marino, G., Foster, G. L.,
728 Hennekam, R., de Lange, G. J., Roberts, A. P., Yu, J., Webster, J. M., & Yokoyama, Y. (2017).
729 Differences between the last two glacial maxima and implications for ice-sheet, $\delta^{18}\text{O}$, and sea-
730 level reconstructions. *Quaternary Science Reviews*, 176, 1–28.
731 <https://doi.org/10.1016/j.quascirev.2017.09.009>
- 732 Rovere, A., Raymo, M. E., Vacchi, M., Lorscheid, T., Stocchi, P., Gómez-Pujol, L., Harris, D.
733 L., Casella, E., O’Leary, M. J., & Hearty, P. J. (2016). The analysis of Last Interglacial (MIS 5e)
734 relative sea-level indicators: Reconstructing sea-level in a warmer world. *Earth-Science Reviews*,
735 159, 404–427. <https://doi.org/10.1016/j.earscirev.2016.06.006>
- 736 Roy, K., & Peltier, W. R. (2015). Glacial isostatic adjustment, relative sea level history and
737 mantle viscosity: Reconciling relative sea level model predictions for the U.S. East coast with
738 geological constraints. *Geophysical Journal International*, 201(2), 1156–1181.
739 <https://doi.org/10.1093/gji/ggv066>
- 740 Roy, K., & Peltier, W. R. (2018). Relative sea level in the Western Mediterranean basin: A
741 regional test of the ICE-7G_NA (VM7) model and a constraint on late Holocene Antarctic
742 deglaciation. *Quaternary Science Reviews*, 183, 76–87.
743 <https://doi.org/10.1016/j.quascirev.2017.12.021>
- 744 Salles, T., Ding, X., Webster, J. M., Vila-Concejo, A., Brocard, G., & Pall, J. (2018). A unified
745 framework for modelling sediment fate from source to sink and its interactions with reef systems
746 over geological times. *Scientific Reports*, 8(1), 5252. <https://doi.org/10.1038/s41598-018-23519-8>
- 747 Sandstrom, M. R., O’Leary, M. J., Barham, M., Cai, Y., Rasbury, E. T., Wooton, K. M., &
748 Raymo, M. E. (2020). Age constraints on surface deformation recorded by fossil shorelines at
749 Cape Range, Western Australia. *GSA Bulletin*. <https://doi.org/10.1130/B35564.1>
- 750 Skrivanek, A., Li, J., & Dutton, A. (2018). Relative sea-level change during the Last Interglacial
751 as recorded in Bahamian fossil reefs. *Quaternary Science Reviews*, 200, 160–177.
752 <https://doi.org/10.1016/j.quascirev.2018.09.033>
- 753 Stirling, C. H., & Andersen, M. B. (2009). Uranium-series dating of fossil coral reefs: Extending
754 the sea-level record beyond the last glacial cycle. *Earth and Planetary Science Letters*, 284(3–4),
755 269–283. <https://doi.org/10.1016/j.epsl.2009.04.045>
- 756 Stirling, C. H., Esat, T. M., Lambeck, K., & McCulloch, M. T. (1998). Timing and duration of
757 the Last Interglacial: Evidence for a restricted interval of widespread coral reef growth. *Earth*

- 759 and *Planetary Science Letters*, 160(3–4), 745–762. [https://doi.org/10.1016/S0012-821X\(98\)00125-3](https://doi.org/10.1016/S0012-821X(98)00125-3)
- 760 Stirling, C. H., Esat, T. M., McCulloch, M. T., & Lambeck, K. (1995). High-precision U-series
761 dating of corals from Western Australia and implications for the timing and duration of the Last
762 Interglacial. *Earth and Planetary Science Letters*, 135(1–4), 115–130.
763 [https://doi.org/10.1016/0012-821X\(95\)00152-3](https://doi.org/10.1016/0012-821X(95)00152-3)
- 764 Thompson, W. G., Allen Curran, H., Wilson, M. A., & White, B. (2011). Sea-level oscillations
765 during the last interglacial highstand recorded by Bahamas corals. *Nature Geoscience*, 4(10),
766 684–687. <https://doi.org/10.1038/ngeo1253>
- 767 Toomey, M., Ashton, A. D., & Perron, J. T. (2013). Profiles of ocean island coral reefs
768 controlled by sea-level history and carbonate accumulation rates. *Geology*, 41(7), 731–734.
769 <https://doi.org/10.1130/G34109.1>
- 770 Whitney, B. B., & Hengesh, J. V. (2015). Geomorphological evidence for late Quaternary
771 tectonic deformation of the Cape Region, coastal west central Australia. *Geomorphology*, 241,
772 160–174. <https://doi.org/10.1016/j.geomorph.2015.04.010>
- 773 Woodroffe, C. D., & Webster, J. M. (2014). Coral reefs and sea-level change. *Marine Geology*,
774 352, 248–267. <https://doi.org/10.1016/j.margeo.2013.12.006>
- 775
- 776